Available online at www.sciencedirect.com
ScienceDirect
International Journal of Heat and Mass Transfer 50 (2007) 1163–1175
International Journal of HEAT and MASS TRANSFER
www.elsevier.com/locate/ijhmt

Three-dimensional numerical study of wavy fin-and-tube heat exchangers and field synergy principle analysis

Y.B. Tao, Y.L. He *, J. Huang, Z.G. Wu, W.Q. Tao

State Key Laboratory of Multiphase Flow in Power Engineering, School of Energy and Power Engineering, Xi'an Jiaotong University, Xi'an, Shaan xi 710049, China

Received 24 October 2005; received in revised form 17 March 2006
Available online 11 December 2006

Abstract

In this paper, 3-D numerical simulations were performed for laminar heat transfer and fluid flow characteristics of wavy fin-and-tube heat exchanger by body-fitted coordinates system. The effect of four factors were examined: *Reynolds* number, fin pitch, wavy angle and tube row number. The Reynolds number based on the tube diameter varied from 500 to 5000, the fin pitch from 0.4 to 5.2 mm, the wavy angle from 0° to 50°, and the tube row range from 1 to 4. The numerical results were compared with experiments and good agreement was obtained. The numerical results show that with the increasing of wavy angles, decreasing of the fin pitch and tube row number, the heat transfer of the finned tube bank are enhanced with some penalty in pressure drop. The effects of the four factors were also analyzed from the view point of field synergy principle which says that the reduction of the intersection angle between velocity and fluid temperature gradient is the basic mechanism for enhance convective heat transfer. It is found that the effects of the four factors on the heat transfer performance of the wavy fin-and-tube exchangers can be well described by the field synergy principle.
© 2006 Elsevier Ltd. All rights reserved.

Keywords: Wavy fin-and-tube heat exchanger; Field synergy principle; Numerical simulation

1. Introduction

Fin-and-tube heat exchangers are employed in a varieties of engineering applications, for example, applications in such areas like air conditioning units, process gas heater and coolers, compressor intercoolers, etc. Since majority of the thermal resistance of fin-and-tube heat exchangers is on the air side, improving air side fin configuration, enhancing its heat transfer is the most effective way to improve the performance of the heat exchangers. One of the conventional methods for enhancing air side heat transfer is the adoption of the wavy and slot fins.

There have been a number of numerical studies on the heat transfer and fluid flow characteristics for two-dimensional corrugated wavy channel flow. Nishimura et al. [1] used the finite element method to study a two-dimensional pulsatile flow in a wavy channel with periodically converging–diverging cross-sections. Xin and Tao [2] numerically analyzed the laminar fluid flow and heat transfer in two-dimensional wavy channels with uniform cross-sectional area. Patel et al. [3,4] numerically investigated the laminar and turbulent boundary layer flows over a wavy wall. Rutledge and Sleicher [5] numerically studied the possibility of improving heat transfer rates by incorporating small corrugations into a two-dimensional channel. Comini and Nonino [6] adopted a simplified two-dimensional approach to deal with convective heat and mass transfer in laminar flows of humid air through wavy finned-tube exchangers.

Experimental studies of heat transfer and pressure drop in two-dimensional corrugated or wavy channels and three-dimensional wavy fin-and-tube heat exchangers have been performed by many researchers. Goldstein and Sparrow [7] used the naphthalene sublimation technique to

* Corresponding author. Tel.: +86 29 82663851; fax: +86 29 82669106.
E-mail address: yalinghe@mail.xjtu.edu.cn (Y.L. He).

0017-9310/$ - see front matter © 2006 Elsevier Ltd. All rights reserved.
doi:10.1016/j.ijheatmasstransfer.2006.03.019

Nomenclature

A	surface or cross-sectional area (m^2)
C_p	specific heat (J/kg K)
D	tube outer side diameter (m)
f	friction factor
F_p	fin pitch (m)
h	heat transfer coefficient (W/m^2 K)
k	thermal conductivity (W/m K)
L	flow length (m)
M	module production
N	the number of control volume or point
n	tube row number
$\vec{n}$	dimensionless unit normal vector
Nu	local Nusselt number, $(h \cdot D)/k$
p	pressure (Pa)
Δp	pressure drop in flow direction (Pa)
Q	heat transfer capacity (W)
Re	Reynolds number based on tube outer side diameter ($U_c D/\upsilon$)
s	arc length along the arbitrary boundary
S	tube row pitch (m)
T	temperature (K)
T_{in}	inlet temperature (K)
T_w	wall temperature (K)
$\overline{T}$	bulk average temperature (K)
$\bar{p}$	bulk average pressure (Pa)
u, v, w	x, y, z velocity components (m/s)
u_{in}	frontal velocity (m/s)
U_c	velocity at the minimum cross-sectional area (m/s)
$\vec{U}$	velocity vector (m/s)
U, V, W	transformed velocity (m/s)
x, y, z	Cartesian coordinates

Greek symbols

α	wavy angle (°)
μ	dynamic viscosity (Pa s)
υ	kinematic viscosity (m^2/s)
ρ	density (kg/m^3)
λ	thermal conductivity (W/m K)
θ	the local intersection angle (°)
ξ, η, ζ	body-fitted coordinates

Subscripts

cal	calculation results
exp	experiment results
in	inlet parameters
m	mean or average value
out	outlet parameters
w	at wall conditions
Γ	boundary segment

determine the local and average heat transfer characteristics for flow in a two-dimensional corrugated wall channel. The effects of rounding of protruding edges of a two-dimensional corrugated wall duct were investigated by Sparrow and Hossfeld [8]. Ali and Ramadhyani [9] experimentally studied the convective heat transfer in the entrance region of two dimensional corrugated channels. Snyder et al. [10] investigated forced-convection heat transfer rates and pressure drops in the thermally fully developed region of a two-dimensional wavy channel. Yoshii [11] presented dry-surface Nusselt number data for two eight-row coils with a wavy pattern . Later, Yoshii et al. [12] reported wet and dry surface data for two wavy-finned cooling coils. Beecher and Fangan [13] experimentally tested 27 fin-and-tube heat exchangers with 21 of them having wavy-fin geometry. Webb [14] used a multiple regression technique to correlate Beecher and Fangan [13] data. An experimental study was conducted by Mirth and Ramadhyani [15] to determine the Nusselt number and friction factor on the air-side of wavy-finned, chilled-water cooling coil. Xin et al. [16] experimentally investigated the air-side heat transfer and pressure drop performances of nine triangular wavy fin-and-tube heat exchanger coils. The Nussult number and friction factor correlations were provided in a wide range of Reynolds number. Wang et al. [17,18] made extensive experiments on the heat transfer and pressure drop characteristics of wavy fin and tube heat exchangers. Somchai and Yutasak [19] experimentally investigated the effect of fin pitch and number of tube rows on the air side performance of herringbone wavy fin and tube heat exchangers.

Jang and Chen [20] numerically studied the heat transfer and fluid flow in a three-dimensional wavy fin-and-tube heat exchanger. The effects of tube row numbers, wavy angles and wavy heights were investigated. Manglik et al. [21] analyzed the effects of fin density on low Reynolds number forced convection in three-dimensional wavy-plate-fin compact channels by numerical simulation.

The foregoing literature review shows that only a little related numerical works on the three-dimensional wavy fin-and-tube heat exchangers have been published in open literatures, and the main emphasis of these studies was placed on the parametric study only. In all the previous studies, these results were just described, or with some explanations from convective heat transfer and fluid flow considerations, not enough in explaining why things happens the way it happened. In this study, the focus will be on the physics of the reasons for enhancement or deterioration of the convective heat transfer with different parameter combinations. In 1998, Guo and his co-workers [22] proposed a novel concept about the enhancement of convective heat transfer for parabolic flow and showed that the reduction of the intersection angle between the velocity and temperature gradient can effectively enhance the heat transfer.

Later, Tao et al. [23,24] demonstrated that this idea is also valid for elliptic flow if the flow Peclet number is not too small. This concept is now called as field synergy principle, since the word "synergy" means cooperative action of two forces or the like [25]. An extension of the field synergy principle to more general transport phenomena was made by He [26] and He et al. [27], and a comprehensive review on the recent development of the study on the field synergy principle was conducted by Tao and He [28], He and Tao [29].

This paper examines the effects of four parameters on the heat transfer and fluid flow of wavy fin-and-tube heat exchangers from the point view of field synergy principle. Numerical simulation for wavy fin-and-tube heat transfer surface is conducted with body-fitted coordinates system and the volume average intersection angle between the velocity and temperature gradient within the computational domain is determined. Then compare the trend of heat transfer and the trend of the average intersection angle with the same parameter to see if the two trends are consistent with the new concept. Numerical results show that the two trends are consistent with the new concept very well.

The details of the field synergy principle can be found from the above-referenced papers, and for the simplicity of presentation, it is not re-stated here.

2. Model description

2.1. Physical model

The schematic diagram of a wavy fin-and-tube heat exchanger is shown in Fig. 1(a). Fig. 1(b) gives a top view of the computation domain of the two-row heat exchanger. Fig. 2 presents the four computation domains of different tube rows (1–4) finned tube banks studied. The actual computation domain was 7.5 times of the original heat transfer zone. The domain was extended 1.5 times of the original heat transfer zone for the entrance section to ensure the inlet uniformity and at the exit of heat transfer region domain was extended 5 times of the original heat transfer zone in order to make sure that the local one-way method

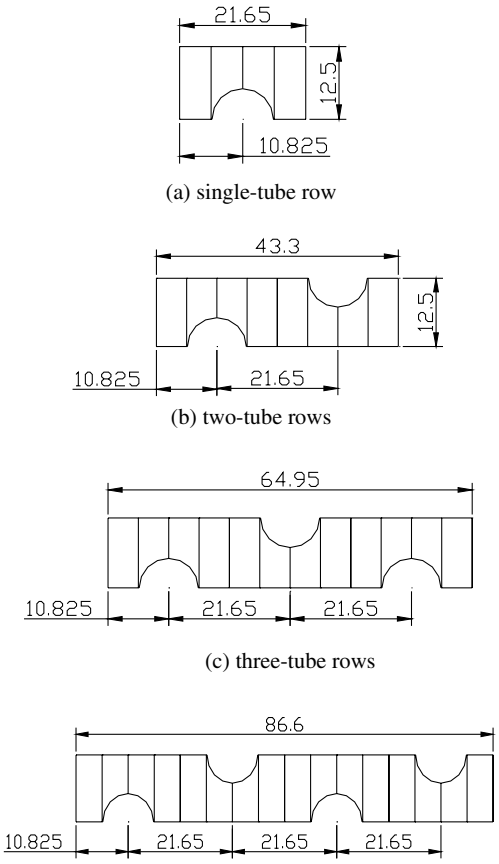

Fig. 2. Schematic of computational domains and geometric parameters of the fin surfaces studied.

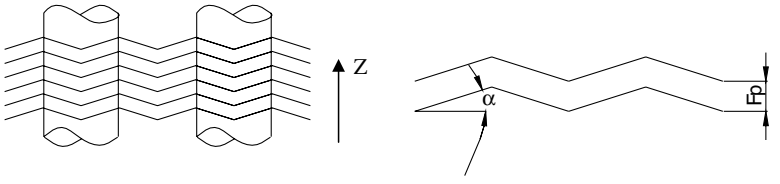

(a) Schematic of wavy fin-and-tube heat exchanger

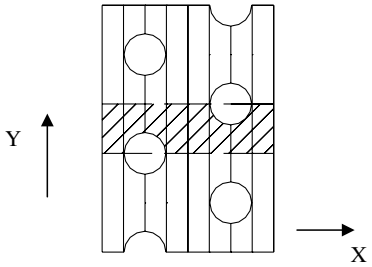

(b) Schematic of computational domain

Fig. 1. Schematic diagram of a wavy fin-and-tube heat exchanger and computation domain.

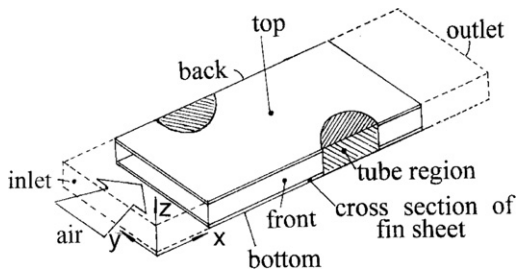

Fig. 3. A pictorial view of the computational domain for two-row case for wavy angle = 0°.

can be used for the numerical treatment of the outer flow boundary condition. In Fig. 3 the pictorial view of the computational domain is presented, where the upstream and downstream parts of the computation domain are not presented in scale with the fin length in order to save the space. In these two parts of the computational domain a much coarser grid distribution was adopted to save the computing resource.

2.2. Grid generation technique

Because of the irregularity of the computational domain, it is difficult to use simple Cartesian coordinates to generate grid. In this paper, the body-fitted coordinates was adopted. The basic idea of the body-fitted coordinate is to numerically generate a curvilinear coordinate system having coordinate lines coincident with each boundary of the real computational domain, regardless of the shapes of these boundaries. This is implemented by solving elliptic partial differential equations. Constant values of one of the curvilinear coordinates are specified as Dirichlet boundary conditions on each boundary. Values of the other coordinates are either specified by a monotonic variation over a boundary as Dirichlet boundary conditions, or determined by Neumann boundary conditions. In the latter case, the curvilinear coordinate lines can be made to intersect the boundary according to some specified conditions, such as being normal or parallel to some given directions. It is also possible to exercise control over the spacing of the curvilinear coordinate lines in the field in order to concentrate lines in regions of expected high gradients. In any case, the numerical generation of the coordinate system is done automatically for any shape boundaries, requiring only the input of points on the boundary.

In order to obtain a grid in the transformed space, a grid system generating method needs to be developed. The simplest equation that could be used to generate the grid is Laplace's equations:

$$\nabla^2 \xi_i = 0, \quad i = 1, 2, 3 \tag{1}$$

The commonly used grid generation techniques are based on the Poisson equation proposed in Thompson et al. [30]. The 3-D Poisson equation in the physical space can be expressed as:

$$\begin{aligned}
&\frac{\partial^2 \xi}{\partial^2 x} + \frac{\partial^2 \xi}{\partial^2 y} + \frac{\partial^2 \xi}{\partial^2 z} = P(\xi, \eta, \varsigma) \\
&\frac{\partial^2 \eta}{\partial^2 x} + \frac{\partial^2 \eta}{\partial^2 y} + \frac{\partial^2 \eta}{\partial^2 z} = Q(\xi, \eta, \varsigma) \\
&\frac{\partial^2 \varsigma}{\partial^2 x} + \frac{\partial^2 \varsigma}{\partial^2 y} + \frac{\partial^2 \varsigma}{\partial^2 z} = R(\xi, \eta, \varsigma)
\end{aligned} \tag{2}$$

where P, Q, R are functions for controlling the spacing between coordinate lines. The above partial differential equations are subject to a set of Dirichlet boundary conditions, such as

$$\begin{bmatrix} \xi \\ \eta \\ \zeta \end{bmatrix} = \begin{bmatrix} \xi_1(x, y, z) \\ \eta_1 \\ \zeta_1(x, y, z) \end{bmatrix}, \quad (x, y, z) \in \Gamma \tag{3}$$

where η_1 is a specified constant, $\xi_1(x, y, z)$ and $\zeta_1(x, y, z)$ are specified monotonic functions on a boundary segment Γ.

The above equations are transformed into the computational space where the Cartesian coordinates are the dependent variables. Then we have

$$\begin{aligned}
&\alpha_{11} x_{\xi\xi} + \alpha_{22} x_{\eta\eta} + \alpha_{33} x_{\zeta\zeta} + 2\alpha_{12} x_{\xi\eta} + 2\alpha_{13} x_{\xi\zeta} \\
&\quad + 2\alpha_{23} x_{\eta\zeta} + J^2 (P x_\xi + Q x_\eta + R x_\zeta) = 0 \\
&\alpha_{11} y_{\xi\xi} + \alpha_{22} y_{\eta\eta} + \alpha_{33} y_{\zeta\zeta} + 2\alpha_{12} y_{\xi\eta} + 2\alpha_{13} y_{\xi\zeta} \\
&\quad + 2\alpha_{23} y_{\eta\zeta} + J^2 (P y_\xi + Q y_\eta + R y_\zeta) = 0 \\
&\alpha_{11} z_{\xi\xi} + \alpha_{22} z_{\eta\eta} + \alpha_{33} z_{\zeta\zeta} + 2\alpha_{12} z_{\xi\eta} + 2\alpha_{13} z_{\xi\zeta} \\
&\quad + 2\alpha_{23} z_{\eta\zeta} + J^2 (P z_\xi + Q z_\eta + R z_\zeta) = 0
\end{aligned} \tag{4}$$

where $\alpha_{jk} = \sum_{m=1}^{3} \beta_{mk} \beta_{mk}$, and β_{mk} is the cofactor of the (m, k) element in the matrix M

$$M = \begin{bmatrix} x_\xi & x_\eta & x_\zeta \\ y_\xi & y_\eta & y_\zeta \\ z_\xi & z_\eta & z_\zeta \end{bmatrix} \quad \text{and} \quad J = \det |M| \tag{5}$$

Thus,

$$\begin{aligned}
\alpha_{11} &= \beta_{11}^2 + \beta_{21}^2 + \beta_{31}^2 \\
\alpha_{22} &= \beta_{12}^2 + \beta_{22}^2 + \beta_{32}^2 \\
\alpha_{13} &= \beta_{13}^2 + \beta_{23}^2 + \beta_{33}^2 \\
\alpha_{12} &= \beta_{11}\beta_{12} + \beta_{21}\beta_{22} + \beta_{31}\beta_{32} \\
\alpha_{13} &= \beta_{11}\beta_{13} + \beta_{21}\beta_{23} + \beta_{31}\beta_{33} \\
\alpha_{23} &= \beta_{12}\beta_{13} + \beta_{22}\beta_{23} + \beta_{32}\beta_{33}
\end{aligned} \tag{6}$$

The transformed boundary conditions are

$$\begin{bmatrix} x \\ y \\ z \end{bmatrix} = \begin{bmatrix} f_1(\xi, \eta_1, \zeta) \\ f_2(\xi, \eta_1, \zeta) \\ f_3(\xi, \eta_1, \zeta) \end{bmatrix}, \quad (\xi, \eta_1, \zeta) \in \Gamma^* \tag{7}$$

where $f_1(\xi, \eta_1, \zeta)$, $f_2(\xi, \eta_1, \zeta)$ and $f_3\ (\xi, \eta_1, \zeta)$ are determined by the known shape of the boundary segment Γ and the specified distribution of ξ thereon. Γ^* is the boundary segment of Γ in the transformed space.

In order to improve the quality of the generated grid system, especially for the parts of wave crest and wave trough, in this paper the final grid systems were generated by the block structured method with body-fitted coordinates [31]. The pictures of the generated grid systems for the fin part will be presented in Section 3.

Now attention is turned to the governing equations and the boundary conditions for the physical problem studied.

2.3. Governing equations

The governing equations in Cartesian coordinates are

Continuity equation:

$$\frac{\partial}{\partial x_i}(\rho u_i) = 0 \tag{8}$$

Momentum equation:

$$\frac{\partial}{\partial x_i}(\rho u_i u_k) = \frac{\partial}{\partial x_i}\left(\mu \frac{\partial u_k}{\partial x_i}\right) - \frac{\partial p}{\partial x_k} \tag{9}$$

Energy equation:

$$\frac{\partial}{\partial x_i}(\rho u_i T) = \frac{\partial}{\partial x_i}\left(\frac{k}{C_p}\frac{\partial T}{\partial x_i}\right) \tag{10}$$

The governing equations in the computational space are

$$\frac{\partial}{\partial \xi}(\rho U) + \frac{\partial}{\partial \eta}(\rho V) + \frac{\partial}{\partial \varsigma}(\rho W) = 0 \tag{11}$$

$$\frac{\partial}{\partial \xi}(\rho U \Phi) + \frac{\partial}{\partial \eta}(\rho V \Phi) + \frac{\partial}{\partial \varsigma}(\rho W \Phi) = \frac{\partial}{\partial \xi}\left(\frac{\alpha}{J}\Gamma^{\Phi}\frac{\partial \Phi}{\partial \xi}\right) + \frac{\partial}{\partial \eta}\left(\frac{\beta}{J}\Gamma^{\Phi}\frac{\partial \Phi}{\partial \eta}\right) + \frac{\partial}{\partial \varsigma}\left(\frac{\gamma}{J}\Gamma^{\Phi}\frac{\partial \Phi}{\partial \varsigma}\right) + JS \tag{12}$$

where U, V, W are velocity component in transformed space.

$$U = \alpha_1 u + \alpha_2 v + \alpha_3 w, \quad V = \beta_1 u + \beta_2 v + \beta_3 w,$$
$$W = \gamma_1 u + \gamma_2 v + \gamma_3 w,$$
$$J = x_\xi y_\eta z_\zeta + x_\eta y_\zeta z_\xi + x_\zeta y_\xi z_\eta - x_\zeta y_\eta z_\xi - x_\eta y_\xi z_\zeta - x_\xi y_\zeta z_\eta \tag{13}$$

2.4. Boundary conditions

The fluid is assumed to be incompressible with constant property and the flow is laminar and in steady state. In order to simplify the generation of grid and the calculation, further simplification is made for the fin. The fin surface is considered to be a constant temperature surface. This implies that the fin efficiency is assumed to be equal to 1. This simplification can also be understood as the assumption of isothermal wall boundary condition.

Inlet boundary condition: $u = u_{\text{in}}, v = w = 0, T = T_{\text{in}}$.
Outlet boundary condition: local one-way method [31].
Front and back boundary condition:
on the tube surface, $u = v = w = 0,\ T = T_{\text{w}}$;
in the rest part,

$$v = 0,\ \frac{\partial u}{\partial y} = 0,\ \frac{\partial w}{\partial y} = 0,\ \frac{\partial T}{\partial y} = 0.$$

Top and bottom boundary condition:
on fin surface, $u = v = w = 0,\ T = T_{\text{w}}$;
in extended surface

$$w = 0,\ \frac{\partial u}{\partial z} = 0,\ \frac{\partial v}{\partial z} = 0,\ \frac{\partial T}{\partial z} = 0.$$

3. Numerical methods and parameter definitions

The governing equations are discretized by using the control volume method [31]. The SIMPLE algorithm is used to ensure the coupling between velocity and pressure.

The definitions of Re, average Nu number and friction factor are as follows.

$$Re = U_{\text{c}} D/\upsilon, \quad Nu = hD/k, \quad f = \Delta p D/[(1/2)\rho U_{\text{c}}^2 L] \tag{14}$$

where U_{c}, υ, and λ are the air velocity in the minimum flow cross-section of the tube row, kinetic viscosity and thermal conductivity, D is the outside diameter of the tube, Δp is the pressure drop along the air flow direction, and L is the fin length along the air flow direction.

The mean temperature and pressure of a cross-section are defined as:

$$\overline{T} = \frac{\int\int_A uT\,\mathrm{d}A}{\int\int_A u\,\mathrm{d}A}, \quad \bar{p} = \frac{\int\int_A p\,\mathrm{d}A}{\int\int_A \mathrm{d}A} \tag{15}$$

The total heat transfer and pressure drop and log-mean temperature difference are expressed as:

$$Q = \dot{m} C_p(\overline{T}_{\text{in}} - \overline{T}_{\text{out}}), \quad \Delta P = \bar{p}_{\text{in}} - \bar{p}_{\text{out}},$$
$$\Delta T = \frac{(T_{\text{w}} - \overline{T}_{\text{in}}) - (T_{\text{w}} - \overline{T}_{\text{out}})}{\ln[(T_{\text{w}} - \overline{T}_{\text{in}})/(T_{\text{w}} - \overline{T}_{\text{out}})]}. \tag{16}$$

The heat transfer coefficient is defined as: $h = Q/(A\Delta T)$.

For the presentation of numerical results in terms of the field synergy principle, the following parameter is introduced:

$$M = \sum |\vec{U}||\text{grad } T|/N \tag{17}$$

where N is the number of the control volume covering the fin region. Obviously, where the intersection angle between velocity and temperature gradient becomes zero, the production of velocity vector and temperature gradient, $|\vec{U}||\text{grad } T|$, is the largest. For simplicity it will be called module production.

The local intersection angle is determined by the following equation:

$$\theta = \cos^{-1}\frac{u\frac{\partial T}{\partial x} + v\frac{\partial T}{\partial y} + w\frac{\partial T}{\partial z}}{|\vec{U}||\text{grad } T|} \tag{18}$$

And from the local intersection angle, the average intersection angle of the computation domain of the fin area can be obtained by using numerical integration,

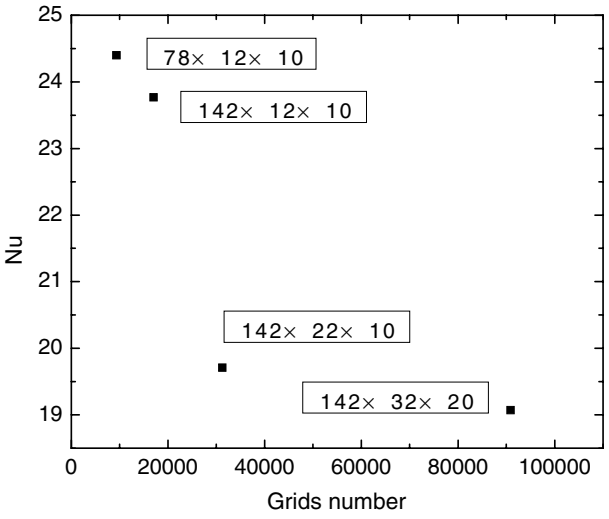

Fig. 4. Variation of the predicted Nusselt number with grid number systems.

$$\theta_m = \frac{\sum \theta_{i,j,k} \mathrm{d}v_{i,j,k}}{\sum \mathrm{d}v_{i,j,k}} \tag{19}$$

where $\mathrm{d}v_{i,j,k}$ is the volume element of the control volume (i,j,k).

The grid independence test has been made. Taking the two-row case as an example. In order to validate the solution independency of the grid number, four different grid systems are investigated. They are $78 \times 12 \times 10$, $142 \times 12 \times 10$, $142 \times 22 \times 10$, $142 \times 32 \times 20$. The predicted averaged Nusselt numbers for the four grid system are shown in Fig. 4. From the figure it can be seen that the solution of the grid system of $142 \times 22 \times 10$ can be regarded as grid-independent. Similar examinations were also conducted for the other three cases. The final grid numbers adopted are $102(x) \times 22(y) \times 10(z)$, $142 \times 22 \times 10$, $182 \times 22 \times 10$, $192 \times 22 \times 10$, respectively for the four cases shown in Fig. 2. The grid systems generated by body-fitted

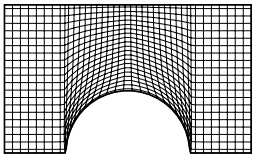

(a) Top view of single-tube row

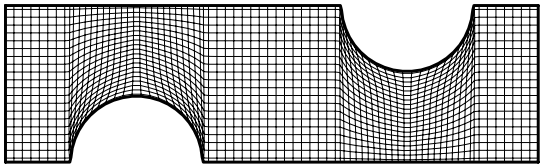

(b) Top view of two-tube row

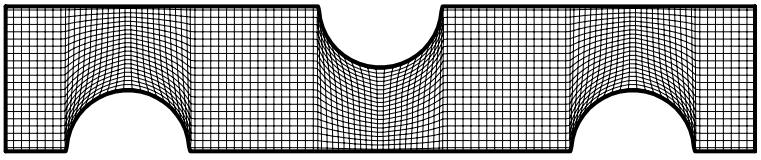

(c) Top view of three-tube row

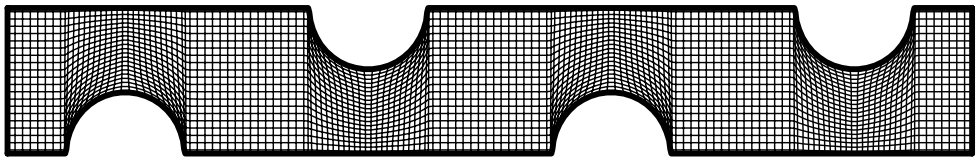

(d) Top view of four-tube row

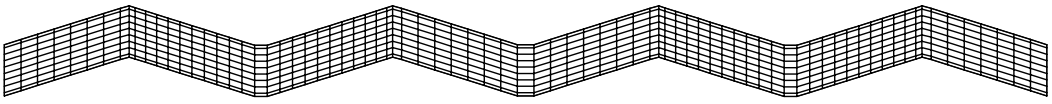

(e) Front view of two-tube row

Fig. 5. Grid systems generated by body-fitted coordinates.

coordinates are illustrated in Fig. 5. Only the fin region is presented in the figure for simplicity.

4. Simulation results and discussions

The effect of the Reynolds number, the fin pitch, the wavy angle, and the tube row number on heat transfer and fluid flow were analyzed by the self-developed code. The major results are presented in the following section.

4.1. Code validation and Re number effect

In order to validate the reliability of the numerical simulation procedure and the self-developed code, numerical simulation was carried out at the same operating conditions and fin geometrical configurations as presented in [16]. The computation is conducted for the two-row case with the tube outside diameter of 10.55 mm, fin pitch 2.096 mm, wavy angle at 17.44°. The *Re* number ranges from 500 to 5000, the corresponding frontal air velocity ranges from 0.464 to 4.64 m/s. The results of the simulation and the comparisons between the simulation and experiment are shown in Fig. 6(a) and (b), where the experimental correlations of the *Nu* and *f* are adopted from [16]:

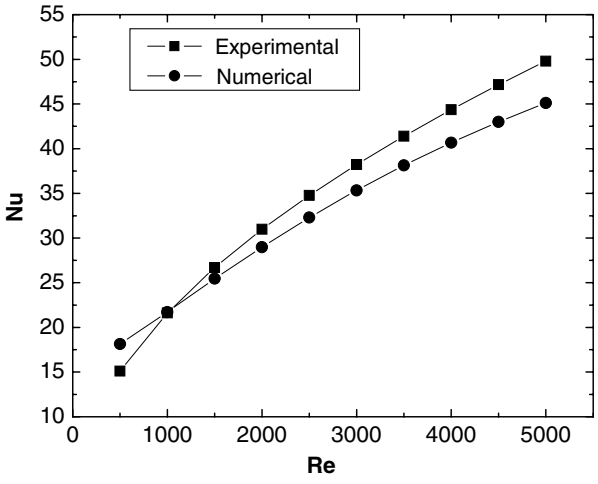

(a) Effect of *Re* on *Nu*

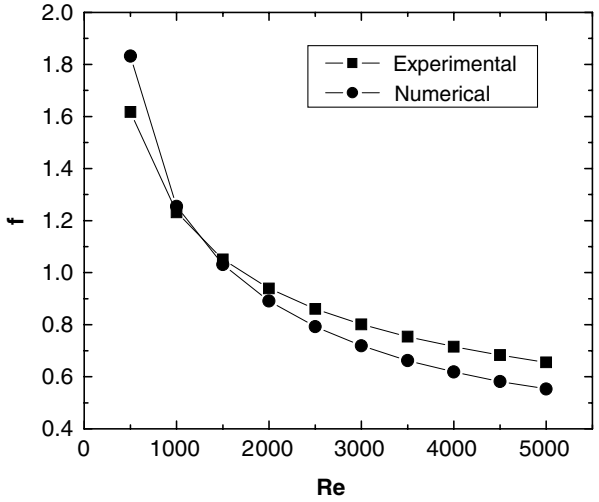

(b) Effect of *Re* on *f*

Fig. 6. Effects of *Re* on *Nu* and *f*.

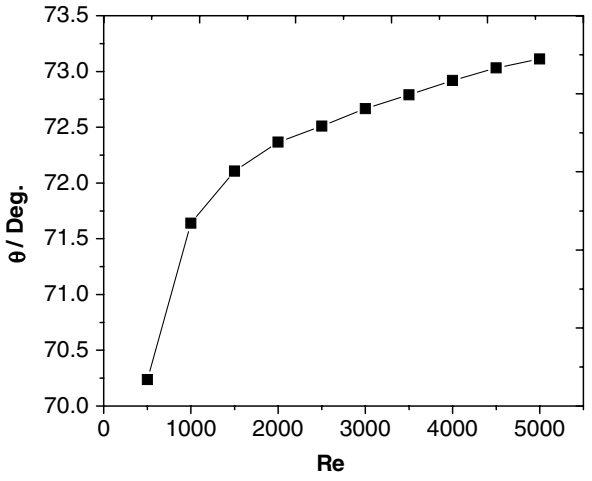

(a) Variation of intersection angle

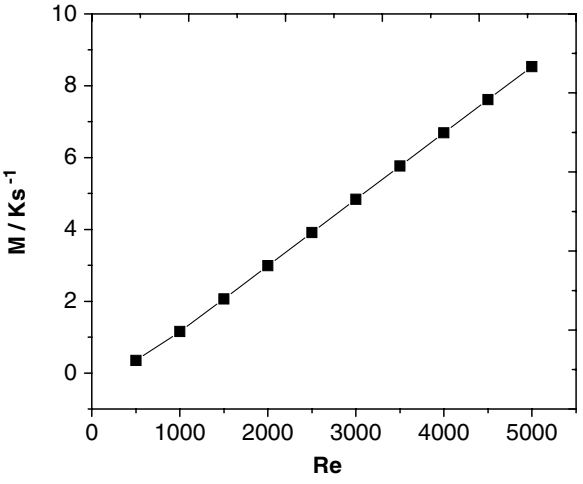

(b) Variation of module production

Fig. 7. Variations of intersection angle and module production with *Re*.

As can be seen from the figures, the agreements are generally good, with the mean deviation in *Nu* and *f* being 8.0% and 9.7%, respectively.

Fig. 7(a) shows the variation of the average intersection angle between velocity and temperature gradient and Fig. 7(b) provides the relation of $M \sim Re$. It can be seen from Fig. 7(a) that the average intersection angle increases with increasing *Re* number, which implies the deterioration of the synergy between velocity and temperature gradient, but Fig. 7(b) indicates that the value of *M* is almost proportional to the *Re* number. Thus, it becomes clear that the decrease of the increasing trend of average *Nu* with *Re* with the increasing of *Re* is resulted from the increase in the intersection angle between the velocity and temperature gradient which means that with the increase in

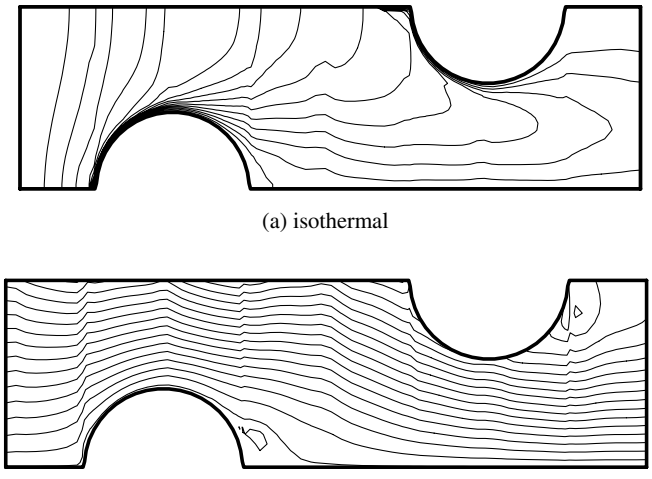

(a) isothermal

(b) streamline

Fig. 8. Distributions of isothermal, streamline for $Re = 1000$ and $\alpha = 17.44°$.

Reynolds number the synergy between velocity and temperature gradient becomes worse and worse.

Fig. 8 presents the local distributions of the temperature, and streamline for the middle cross-section in the x–y plane between the upper and lower sides of the fin for $Re = 1000$ and the wavy angle $\alpha = 17.44°$. It can be seen from the figure that in the inlet part of the fin surface the isotherms are more or less normal to the local streamlines, indicating a very good synergy between the velocity and temperature field. In the rest part of the fin surface, the synergy in some part of the region becomes worse, characterized by the almost parallel distributions of the streamlines and the isotherms, and in the backward part of the two tubes, flow separation occurs and vortex is formed. Thus, from the synergy point of view the local heat transfer intensity basically decreases streamwisely. Such variation pattern is qualitatively the same for the different cases studied in this paper.

4.2. Fin pitch effect

For examining the effect of fin pitch, the two-tube-row configuration is adopted. The fin pitch varies from 0.4 to 5.2 mm with $Re = 1000$, wavy angle at 17.44° and the other parameters kept the same.

Fig. 9(a) shows the relation of the Nu number and the fin pitch. It can be seen that the Nu number reaches the maximum at the fin pitch of 0.6 mm. Departure away from this fin pitch will leads to the decrease of the average Nu number. When the fin pitch is larger than 2.8 mm, the fin pitch has little effect on the average Nu number. The effect of fin pitch on the friction factor is presented in Fig. 9(b), which indicates that with the increase of the fin pitch, f will always decrease, and when fin pitch is larger than 2.8 mm, the fin pitch has little effect on f either.

The field synergy presentations are provided in Fig. 10. It can be concluded from the figure that the average intersection angle almost equal to the same value when the fin pitch is less than 0.6 mm. The increase of fin

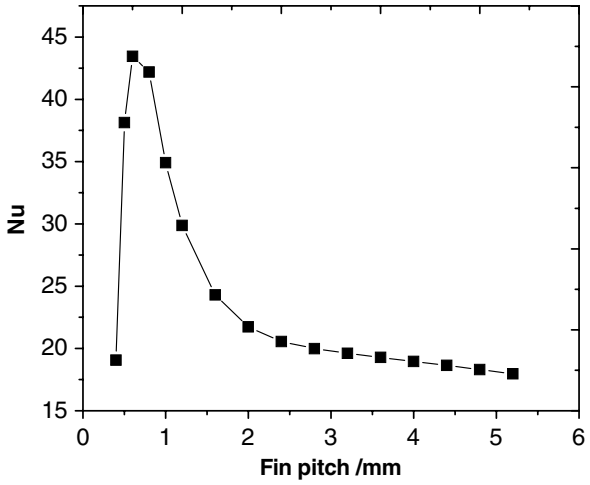

(a) Variation of average Nu with fin pitch

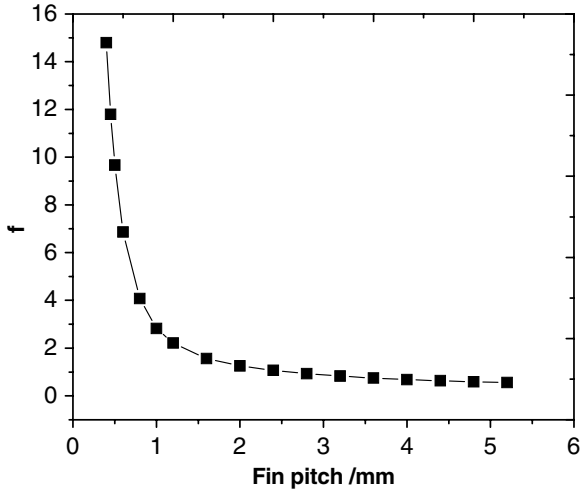

(b) Variation of average f with fin pitch

Fig. 9. Variations of average Nu and f with fin pitch.

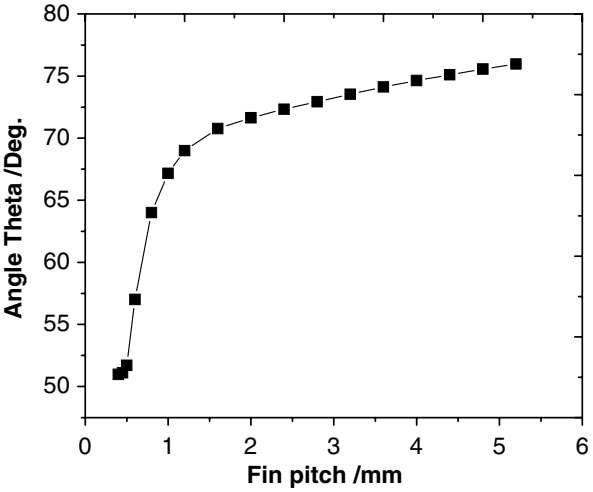

Fig. 10. Variations of average intersection angle with fin pitch.

pitch from this value leads to the increase in the angle, which is very sensitive to the fin pitch close to this value, and once the fin pitch is greater than 1.5 mm the dependence becomes weaker with increasing fin pitch. Such variation pattern of $\theta_m \sim F_p$ is basically consistent with the variation of $Nu \sim F_p$ shown in Fig. 9(a). It is noticed that the variation of Nu with the fin pitch shown in Fig. 9(a) seems a little too abrupt. The computations were repeated for several times and the same results were obtained. One possible reason is the isothermal assumption of the fin surface. In practical situation the fin surface temperature distribution also depends on the flow velocity. The variation of the fin pitch affects the flow field and hence the fin surface temperature distribution, which in turn affects the fluid temperature distribution. Such mutual influences may lead to a more mild variation of the heat transfer coefficient and intersection angle vs. fin pitch. Efforts are now being paid to solve the temperature fields in both fluid and fin sheet in a conjugated way in our group and the results will be reported elsewhere.

The distribution of the temperature and the streamline at the middle cross-section for fin pitch equals 1.0 mm and 5.2 mm are provided in Fig. 11. From the figure it can be clearly observed that the velocity–temperature synergy for $F_p = 5.2$ mm is worse than that of 1.0 mm. In addition, for the case of $F_p = 5.2$ mm, two vortices occur at the backward of the two tubes, which further deteriorate the heat transfer.

4.3. Wavy angle effect

The effects of the wavy angle on the average Nu number and f factor are shown in Fig. 12(a) and (b). The wavy angle varies from 0° to 50° with $Re = 1000$, fin pitch 2.0 mm and the other parameters remain the same.

Fig. 12(a) shows the relation of the Nu number and the wavy angle. It can be seen that the Nu number increases with the increase of wavy angle, and the trend becomes stronger at larger wavy angles. Fig. 12(b) shows the relation of $f \sim \alpha$ which has the same variation trend as $Nu \sim \alpha$.

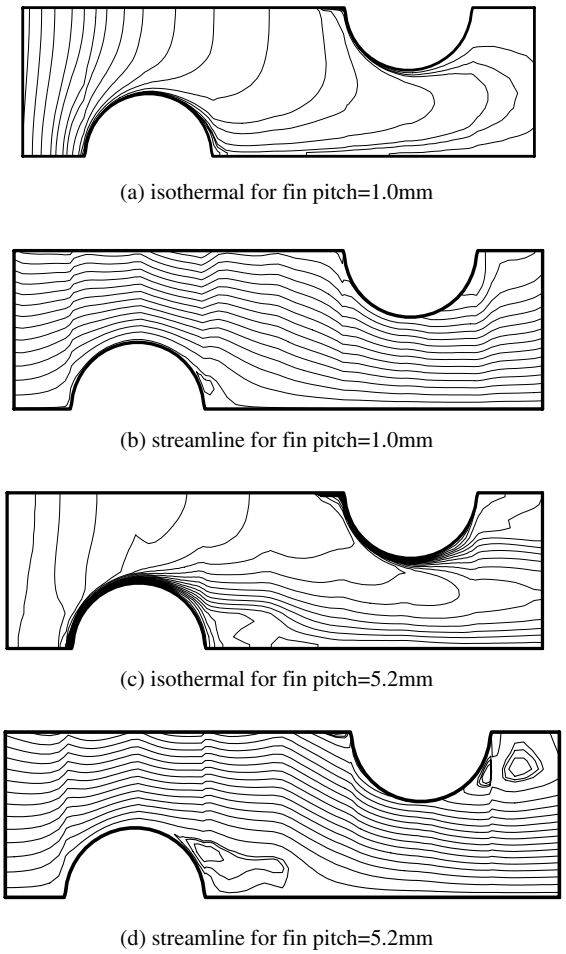

(a) isothermal for fin pitch=1.0mm

(b) streamline for fin pitch=1.0mm

(c) isothermal for fin pitch=5.2mm

(d) streamline for fin pitch=5.2mm

Fig. 11. Distributions of isothermal, streamline for fin pitch = 1.0mm and 5.2 mm.

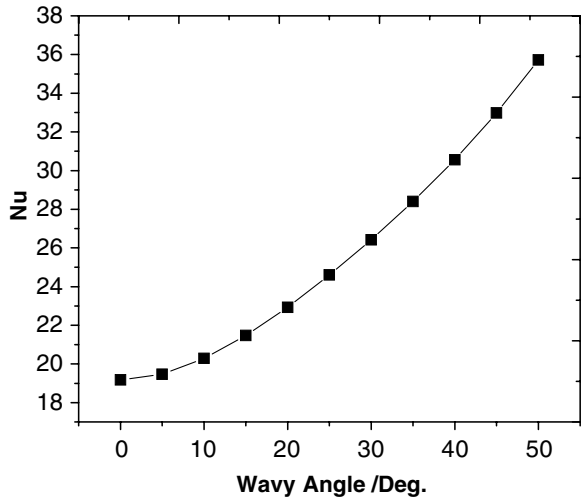

(a) Effect of wavy angle on Nu

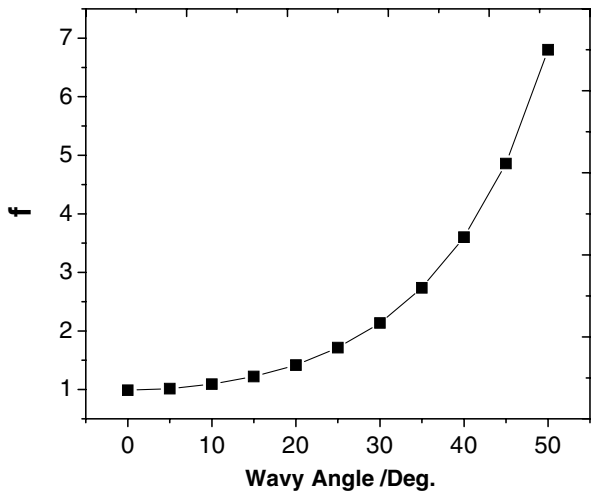

(b) Effect of wavy angle on f

Fig. 12. Effects of wavy angle on Nu and f.

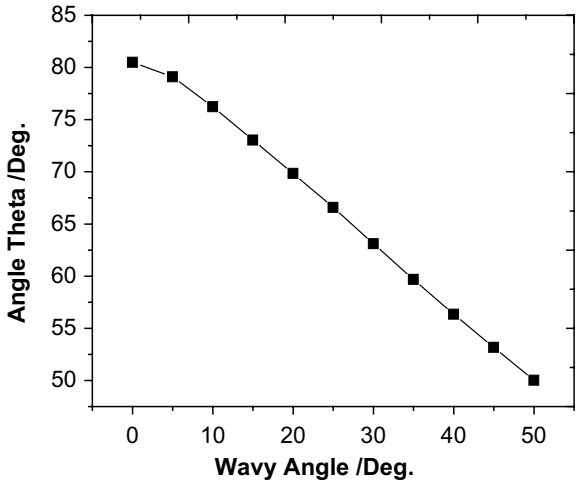

(a) Variation of average intersection angle

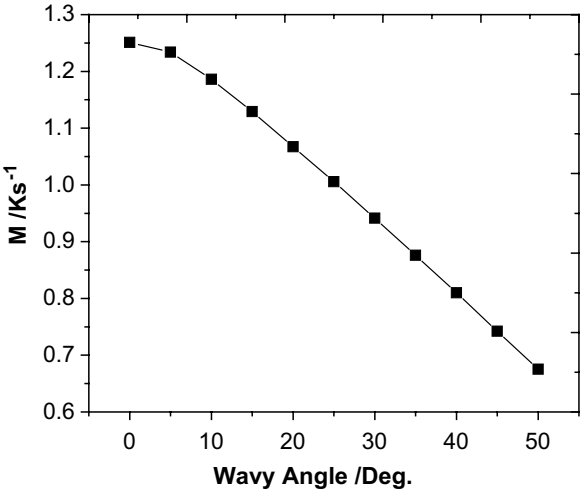

(b) Variation of module production

Fig. 13. Variations of average intersection angle and module production with wavy angle.

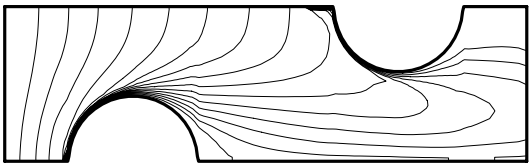

(a) isothermal for wavy angle=0°

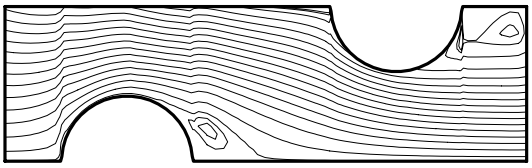

(b) streamline for wavy angle=0°

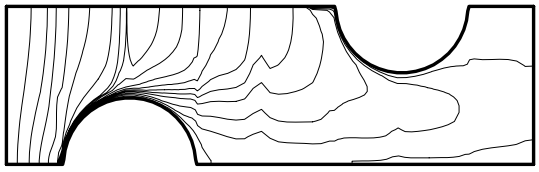

(c) isothermal for wavy angle=30°

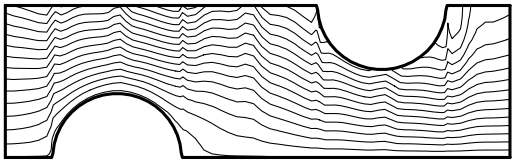

(d) streamline for wavy angle=30°

Fig. 14. Distributions of isothermal, streamline for wavy angle = 0° and 30°.

Fig. 13(a) presents the variation of the average intersection angle between velocity and temperature gradient and Fig. 13(b) provides the relation of $M \sim Re$. From Fig. 13(a) it can be seen that the average intersection angle decreases with increasing wavy angles, which implies the better synergy between velocity and temperature gradient, and Fig. 13(b) indicates that the value of M decreases with the increasing of the wavy angle too. And from further comparison between the effects of intersection angle decrease and the module production decrease, it can be found that the positive effect resulted from the intersection angle decrease is much larger than the negative effect of the module production decrease. Thus, it becomes clear that the increase of average Nu with the increase of α is resulted from the improvement of synergy between velocity and temperature gradient.

The distribution of the temperature and the streamline at the middle cross-section for wavy angle equals 0° and 30° are provided in Fig. 14. It can be observed from the figure that at $\alpha = 30°$ the synergy becomes better and the two vortices occurring at $\alpha = 0°$ disappear, leading to a better heat transfer intensity.

4.4. Tube row number effect

For examining the effect of tube row number on the heat transfer and flow characteristics of the wavy fin-and-tube heat exchanger, the Re number was chosen as 1000, fin pitch of 2.0 mm and wavy angle at 17.44°.

Fig. 15(a) shows the variation of the average Nu number with the tube row number n. The Nu number decreases with the increase of tube row number. The difference of Nu number of two and three rows is very distinct, but the difference between three and four rows is very subtle. These are fully consistent with available test results [16]. The effect of tube row number on f is shown in Fig. 15(b). According to the figure, the f decreases with the increase of tube row number n. The difference of f factor of two and three rows is very subtle, but the difference between one and two rows is very distinct.

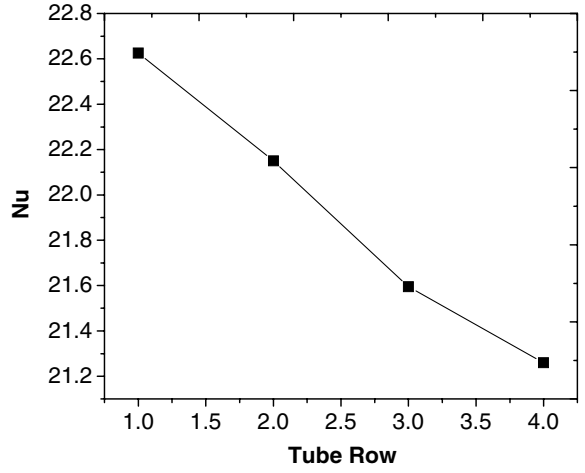

(a) Variation of $Nu \sim n$

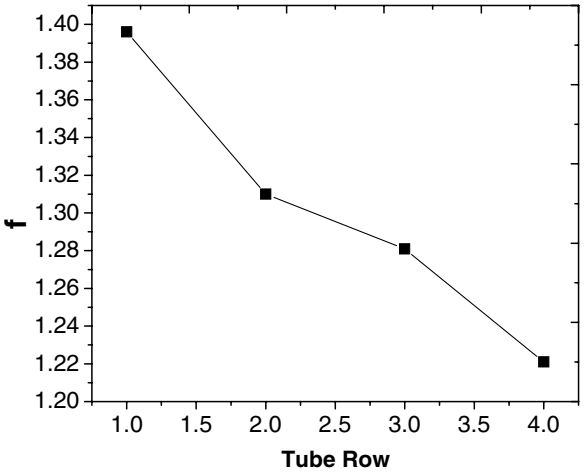

(b) Variation of $f \sim n$

Fig. 15. Variations of Nu and f with tube row number.

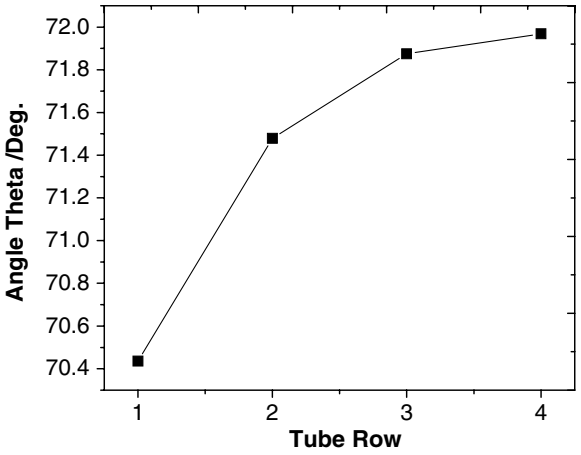

(a) Variation of $\theta \sim n$

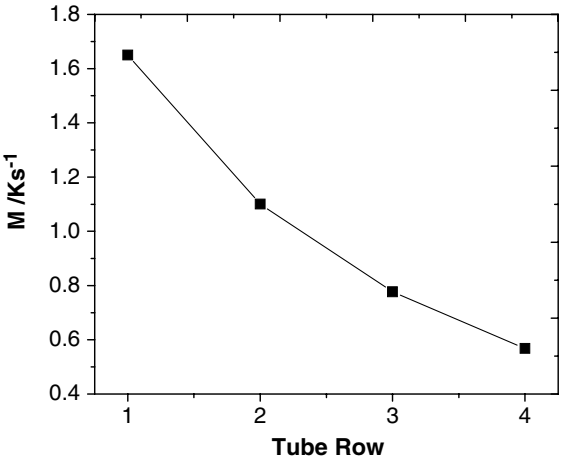

(b). Variation of $M \sim n$

Fig. 16. Variations of average intersection angle and module production with tube row number.

The variation of intersection angle with tube row number is provided in Fig. 16(a). The angle increase with the increasing tube row number, and after $n \geqslant 3$, the effect of n on θ is small. The product of modules of velocity and temperature gradient is shown in Fig. 16(b). With the tube row number increasing, M decreases and the decrease trend slows down gradually. These explains why the average Nu number decrease with the tube row number increase and why the decrease tendency slows down after $n \geqslant 3$. The above findings show that the smaller the tube row number the better the field synergy (for tube row $n > 1$), and the better the heat transfer performance. So in practical applications, the tube row number less than 3 should be recommended.

Attention is now turned to the velocity distribution in the corrugated channel with tube inserted. The velocity distributions in x–z plane at three y-positions are selected to show the major characters of the three-dimensional flow. In Fig. 17 such distributions are provided for the two-row tube case at $Re = 1000$ and $\alpha = 17.44°$. In all the figures presented the dimensions are scale. Fig. 17(a)–(c) presented the velocity in x–z plane at front, middle and back section. In order to improve the resolution, in Fig. 17(d)–(g) the velocity distributions in the front and middle section are separated into two parts. From these figures, following features may be noted. First, in the backside of the two tubes vortices are formed, characterized by the small values of velocities in that region. Second, in the middle section where there is not any inserted tube, the flow field is similar to that in a corrugated channel, characterized by the continuing change of the flow direction and part of the corrugated surface is impinged by the oncoming flow. Third, by carefully inspecting the flow fields in the middle section, it can be found that for the four corrugations, in the first part of the first corrugation, second part of the second corrugation and second part of the third corrugation the main stream is basically parallel to the channel, while in the rest of the corrugated channel, more or less impingement occurs either at the top wall or at the bottom wall. When impingement occurs at one wall the

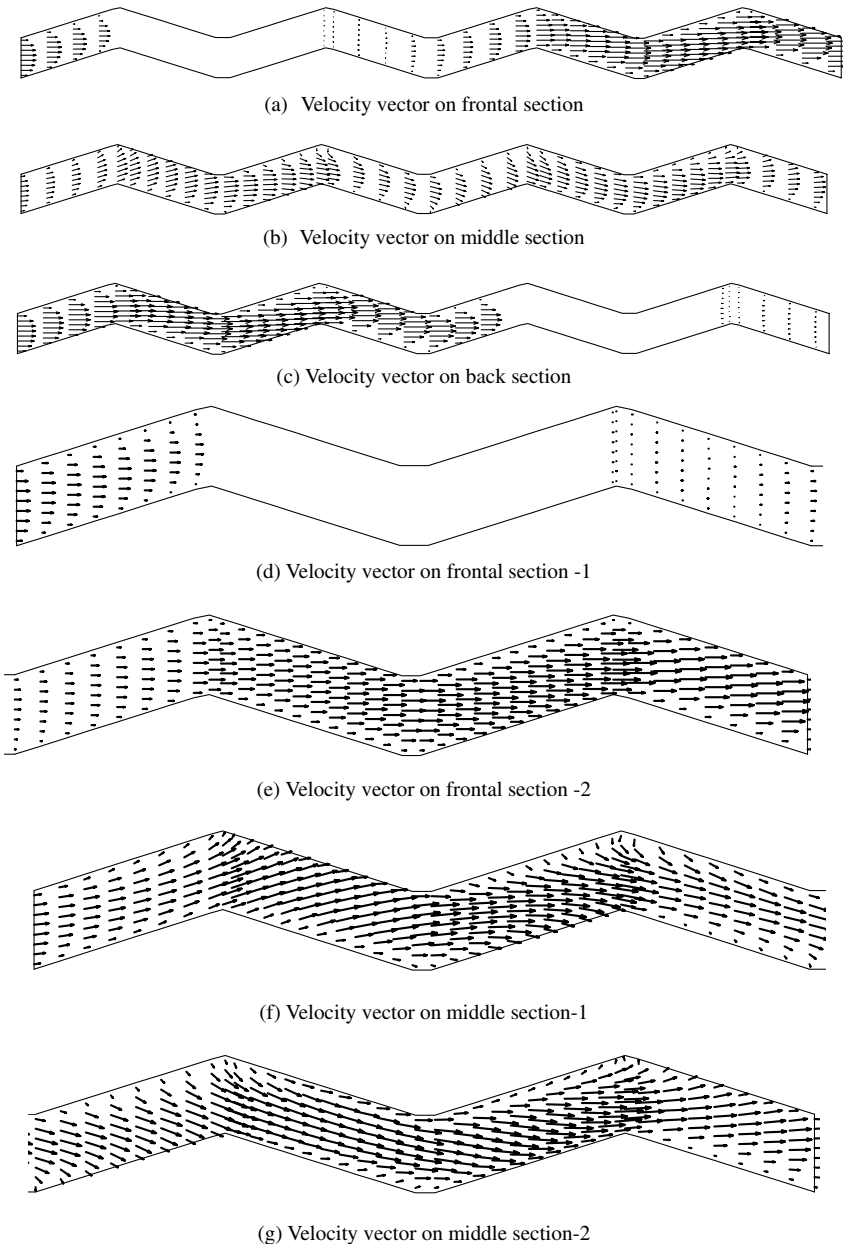

(a) Velocity vector on frontal section

(b) Velocity vector on middle section

(c) Velocity vector on back section

(d) Velocity vector on frontal section -1

(e) Velocity vector on frontal section -2

(f) Velocity vector on middle section-1

(g) Velocity vector on middle section-2

Fig. 17. Velocity distributions at different x–z sections for two-row case.

fluid leave the opposite wall. For the case studied, no strong recirculation is observed.

5. Conclusions

In this paper, 3-D numerical simulations are conducted to explore the effect of the Reynolds number, fin pitch, wavy angle and the tube row number on the heat transfer and fluid flow characteristics of wavy fin-and-tube heat transfer surfaces. The numerical results are analyzed from the point view of the field synergy principle. The numerical results obtained in this study show that the heat transfer performance of the wavy fin-and-tube heat exchanger can well be described by the field synergy principle. The following conclusions can be made.

(1) The increase of *Re* number leads to the increase of the *Nu* number and the decrease of the *f*. The enhancement of heat transfer is due to the increase of the module product of velocity and temperature gradient. However, the synergy between the velocity and the temperature gradient becomes worse and worse with the increase of the Reynolds number, leading to a less increasing tendency of *Nu* with *Re*.
(2) There exists an optimum fin pitch at which the *Nu* number is the maximum, but *f* always decreases with the increase of fin pitch. The average intersection angle shows an asymptotic tendency with the increase of fin pitch, leading to the insensitivity of the *Nu* number with the increase of fin pitch beyond a certain value of the fin pitch.

(3) Both the *Nu* number and *f* increase with the increase of wavy angle, and the increasing trend of *Nu* number and *f* increases with the wavy angle increasing. The increase of average *Nu* is resulted from the decrease in the intersection angle between the velocity and temperature gradient.
(4) The average *Nu* number and *f* factor decreases with the increase of tube row number. The less the tube row number, the better the field synergy. For practical applications, a tube row number less than 3 is recommended from the heat transfer performance by the field synergy principle.

Acknowledgements

The present work is supported by the National Science Fund for Distinguished Young Scholars from the National Natural Science Foundation of China (No. 50425620), and the Key grant Project of Chinese Ministry of Education (No. 306014).

References

[1] T. Nishimura, T. Yoshino, Y. Kawamura, Numerical flow analysis of pulsatile flow in a channel with symmetric wavy walls at moderate Reynolds numbers, J. Chem. Eng. Jpn. 20 (5) (1987) 479–485.
[2] R.C. Xin, W.Q. Tao, Numerical prediction of laminar flow and heat transfer in wavy channels of uniform cross-section area, Numer. Heat Transfer 14 (1988) 465–481.
[3] V.C. Patel, J.T. Chon, J.Y. Yoon, Laminar flow over wavy walls, Trans. ASME 113 (1991) 574–578.
[4] V.C. Patel, J.T. Chon, J.Y. Yoon, Turbulent flow over wavy walls, J. Fluids Eng. 113 (1991) 578–583.
[5] J. Rutledge, C.A. Sleicher, Direct simulation of turbulent flow and heat transfer in a channel. Part II: a Green's function technique for wavy walls, Commun. Numer. Meth. Eng. 10 (1994) 489–496.
[6] G. Comini, C. Nonino, S. Savino, Convective heat and mass transfer in wavy finned-tube exchangers, Convect. Heat Mass Transfer (2002) 733–755.
[7] L. Goldstein, J.M.E. Sparrow, Heat/mass transfer characteristics for flow in a corrugated wall channel, J. Heat Transfer 99 (1977) 187–195.
[8] E.M. Sparrow, L.M. Hossfeld, Effect of rounding of protruding edges on heat transfer and pressure drop in a duct, Int. J. Heat Mass Transfer 27 (10) (1984) 1715–1723.
[9] M.M. Ali, S. Ramadhyani, Experiments on convection heat transfer in corrugated channels, Exp. Heat Transfer 5 (1992) 175–193.
[10] B. Snyder, K.T. Li, R.A. Wirtz, Heat transfer enhancement in a serpentine channel, Int. J. Heat Mass Transfer 36 (12) (1993) 2965–2976.
[11] T. Yoshii, Transient testing technique for heat exchangers fin surfaces, Heat Transfer Jpn. Res. 1 (3) (1972) 51–58.
[12] T. Yoshii, M. Yamamoto, T. Otaki, Effects of dropwise condensate on wet surface heat surface heat transfer for air cooling oils, in: Proceedings of the 13th International Congress of Refrigeration, 1973, pp. 285–292.
[13] D.T. Beecher, T.J. Fagan, Effects of fin pattern on the air side heat transfer coefficient in plate finned-tube heat exchangers, ASHRAE Trans. 93 (2) (1987) 1961–1984.
[14] R.L. Webb, Air side heat transfer correlations for flat and wavy plate fin-and-tube geometries, ASHRAE Trans. 96 (2) (1990) 445–449.
[15] D.R. Mirth, S. Ramadhyani, Correlation for predicting the air-side Nusselt numbers and friction factor in chilled water cooling coils, Exp. Heat Transfer 7 (1994) 143–162.
[16] R.C. Xin, H.Z. Li, H.J. Kang, W. Li, W.Q. Tao, An experimental investigation on heat transfer and pressure drop characteristics of triangular wavy fin-and-tube heat exchanger surfaces, J. Xi'an Jiaotong Univ. 28 (2) (1994) 77–83.
[17] C.C. Wang, W.L. Fu, C.T. Chang, Heat transfer and friction characteristics of typical wavy fin-and-tube heat exchangers, Heat Transfer Friction Character. 14 (1997) 174–186.
[18] C.C. Wang, J.Y. Jang, N.F. Chiou, A heat transfer and friction correlation for wavy fin-and-tube heat exchangers, Int. J. Heat Mass Transfer 42 (1999) 1919–1924.
[19] W. Somchai, C. Yutasak, Effect of fin pitch and number of tube rows on the air side performance of herringbone wavy fin and tube heat exchangers, Energy Convers. Manage. 46 (2005) 2216–2223.
[20] J.Y. Jang, L.K. Chen, Numerical analysis of heat transfer and fluid flow in a three-dimensional wavy-fin and tube heat exchanger, Int. J. Heat Mass Transfer 40 (16) (1997) 3981–3990.
[21] R.M. Manglik, J.H. Zhang, A. Muley, Low Reynolds number forced convection in three-dimensional wavy-plate-fin compact channels: fin density effects, Int. J. Heat Mass Transfer 48 (2005) 1439–1449.
[22] Z.Y. Guo, D.Y. Li, B.X. Wang, A novel concept for convective heat transfer enhancement, Int. J. Heat Mass Transfer 41 (1998) 2221–2225.
[23] W.Q. Tao, Z.Y. Guo, B.X. Wang, Field synergy principle for enhancing convective heat transfer-its extension and numerical verifications, Int. J. Heat Mass Transfer 45 (2002) 3849–3856.
[24] W.Q. Tao, Y.L. He, Q.W. Wang, Z.G. Qu, F.Q. Song, A unified analysis on enhancing single phase convective heat transfer with field synergy principle, Int. J. Heat Mass Transfer 45 (24) (2002) 4871–4879.
[25] D.B. Guralnik, Editor-in -chief, WEBSTER'S New Word Dictionary of the American Language, second college ed., William Collins Publishers, Inc., Cleveland, 1979, p. 1444.
[26] Y.L. He, Theoretical and experimental investigations on the performance improvements of split-stirling cryocooler and pulse tube refrigerator, Ph.D. Thesis, Xi'an Jiaotong University, 2002.
[27] Y.L. He, M. Wu, W.Q. Tao, Z.Q. Chen, Improvement of the thermal performance of pulse tube refrigerator by using a general principle for enhancing energy transport and conversion processes, J. Appl. Therm. Energy 24 (2004) 79–93.
[28] W.Q. Tao, Y.L. He, Field synergy principle and its application in enhancing convective heat transfer and improving performance of pulse tube refrigerator, Part I, J. Xi'an Jiaotong Univ. 36 (2002) 1101–1105.
[29] Y.L. He, W.Q. Tao, Field synergy principle and its application in enhancing convective heat transfer and improving performance of pulse tube refrigerator, Part II, J. Xi'an Jiaotong Univ. 36 (2002) 1106–1110.
[30] J.F. Thompson, F.C. Thames, C.W. Mastin, Automatic numerical generation of body-fitted curvilinear coordinate system for field containing any number of arbitrary two-dimensional bodies, J. Compt. Phys. 15 (1974) 299–319.
[31] W.Q. Tao, Numerical Heat Transfer, second ed., Xi'an Jiaotong University Press, Xi'an, 2001.